energies

Article

Techno-Economic Assessment of CPVT Spectral Splitting Technology: A Case Study on Saudi Arabia

Cesar Lucio *, Omar Behar and Bassam Dally

CCRC, King Abdullah University of Science and Technology (KAUST), Thuwal 23955, Saudi Arabia; omar.behar@kaust.edu.sa (O.B.); bassam.dally@kaust.edu.sa (B.D.)
* Correspondence: cesar.cifuentes@kaust.edu.sa

Abstract: Concentrating PV thermal (CPVT) collector with spectral splitting technology is a promising solution for heat and electricity production. To extend the use of this technology, a novel and cost-effective CPVT collector for harsh environments, such as those in Saudi Arabia, is presented and evaluated using theoretical energy, economy, and environmental analysis. Two questions are answered in this study, namely: which is the best operation strategy, and which is the best energy storage technology for CPVT. The potential of using a CPVT under the climate conditions of six cities in Saudi Arabia is also evaluated. It is found that a heat/electricity production strategy and a thermal energy storage are the most suitable for the CPVT technology. The economic assessment shows a levelized cost of electricity (LCOE) of \$0.0847/kWh and a levelized cost of heat (LCOH) of \$0.0536/kWh when water is used as a spectral filter, and a LCOE of \$0.0906/kWh and a LCOH of \$0.0462/kWh when ZnO nanoparticles are added. The CO_2-equivalent emissions in a 20 MW CPVT plant are cut from 5675 tonnes to 7822 tonnes per year for Saudi Arabian weather and present power generation conditions.

Keywords: CPVT; spectral filtering; solar energy

Citation: Lucio, C.; Behar, O.; Dally, B. Techno-Economic Assessment of CPVT Spectral Splitting Technology: A Case Study on Saudi Arabia. *Energies* **2023**, *16*, 5392. https://doi.org/10.3390/en16145392

Academic Editor: Armando Oliveira

Received: 28 May 2023
Revised: 4 July 2023
Accepted: 12 July 2023
Published: 14 July 2023

1. Introduction

Solar energy can play an important role in a sustainable worldwide energy supply to address carbon emission and climate change. The range and the applications of solar energy conversion devices have expanded dramatically in recent years, with the objective of reducing reliance on fossil fuels. Solar energy can be converted into useful energy using thermal and photovoltaic (PV) collectors.

Traditional PV collectors convert part of the solar spectrum into electricity (typical efficiency of traditional PV panels is about 20%). The rest of the energy received by the PV panel is converted into heat, decreasing its performance. This constraint has led research groups all around the world to seek ways to use the solar radiation that cannot be converted by the PV cells into electricity, in other words, to be able to exploit the entire solar spectrum while preventing photovoltaic cell from overheating.

In this regard, spectrum beam splitting (SBS) has been the technique that has undergone the greatest progress in recent years. It employs filters that split the incoming solar radiation into different wavelengths. The solar radiation within the spectral window, useful for the photovoltaic effect, is directed to PV panels, while the unutilized energy by the PV panels is directed and absorbed by a heat transfer fluid (HTF) to generate heat. The PV panel and the solar thermal collector is combined into a single unit, which is known as, concentrating solar photovoltaic thermal (CPVT) collector.

There are three main methods to split solar radiation into different ranges of wavelengths: interference filtering, use of semi-transparent PV panels, and selective absorption. The challenge of using interference filters is their complicated manufacturability and high cost [1,2]. Some limitations of the semi-transparent PV panels include development of semi-transparent electrodes [3], insulation issues [4] and that some materials are made semi-transparent by reducing the semiconductor's layer thickness; however, doing so results in a reduction in performance [5]. Alternatively, selective absorbers employing HTFs could be a more affordable approach. An HTF that is transparent to the desired wavelengths for PV cells is located in front of them, letting those wavelengths be transmitted to the cells. The HTF is highly absorbing in the rest of the spectrum [2]. From the economic point of view, selective absorption is a cost-effective technique since the working fluid can be water [6].

Several researchers have been working to develop the CPVT technology. One of the first studies was performed by Soule [7], who proposed, in 1987, a CPVT using dome-shaped linear Fresnel lenses as the concentrator with a dielectric-Au-dielectric multilayer filter. The system produced electricity, low-temperature thermal energy (50–70 °C), and high-temperature thermal energy (150–250 °C). The corresponding efficiencies are 9.5%, 41.9%, and 17.8%, respectively. A CPVT with SBS and a parabolic trough collector (PTC) has been proposed by Zhang et al. [8]. The system achieved a maximum electrical efficiency of 22.64%. Some studies showed that a CPVT with PTC can reach an overall thermal efficiency of 70% and an overall electrical efficiency of 25%, while a system with a Linear Fresnel Collector (LFC) can achieve a thermal efficiency of more than 60% and an electrical efficiency of more than 20% [9].

Ling et al. [10] investigated a CPVT with LFC and a selective filter and found a levelized cost of electricity (LCOE) of $0.20/kWh. Recently, Liew et al. [11] proposed a photovoltaic/concentrated solar power hybrid plant to increase the performance of a concentrated solar power plant currently operating in California, USA. The proposed hybrid system performed 9% better than the actual one and was also 4% more efficient than the virtual photovoltaic-alone scenario.

Instead of using solid filters for SBS, liquid absorptive filters can be used and have several advantages [12]. The absorptive liquid is often inexpensive and can perform numerous functions: it absorbs the unused spectral solar irradiance by PV cells; thermal energy can be transported and stored by absorptive fluids; and it could be used as the coolant of PV modules to extract the dissipated heat from the solar cells. Sabry et al. [13] theoretically demonstrated that an ideal liquid filter, which matches the spectral response of silicon solar cells, significantly reduces the solar cells' operating temperature and increases their efficiency by 30%. The performance of a combined liquid and solid absorptive filter on a compact CPVT receiver for an LFC was investigated by Manfred et al. [14]. They found that, for Seville (Spain), the receiver can achieve an electrical efficiency of up to 6.2% and a thermal efficiency of up to 61.2%.

Advances in nanotechnology have resulted in nanoparticles that can selectively filter solar radiation and can be added to a base fluid to modify its optical characteristics. Meraje et al. [15] designed and validated a CPVT based on LFC and a nanofluid spectrum splitting filter. They evaluated several volume concentrations of ZnO nanoparticles. The closest spectrum match with a silicon solar cell was determined to be 0.00089 vol%. Recently, Barthwal et al. [16] examined the utilization of deionized water and ZnO nanoparticles as optical filters in a compound parabolic-concentrate-based CPVT. They evaluated it for conditions in New Delhi (India) and concluded that the cell temperature was kept near the standard test. Wang et al. [17] studied a CPVT with compact LFC and Ag/$CoSO_4$-PG nanofluids. The performance estimation showed that the PV module has a photoelectric efficiency of 30.2%, and the receiver has a thermal efficiency up to 49.3%.

In terms of the applications for CPVT, Su et al. [18] investigated the feasibility of applying CPVT to boost biomethane generation in anaerobic digestion via biogas upgrading. They also proposed the use of CPVT for trigeneration (heat, cooling, and electricity) [19]. At Tucson (United States), Fernandes et al. [20] carried out a simulation for a small-scale nanofluid spectral filtering CPVT for domestic applications. The possibility of using CPVT for water desalination has also been investigated by several authors as reviewed by Anand. et al. [21]. Another recent application of a CPVT was proposed by Youssef et al. [22].

While many of the previous studies have investigated different types of CPVT collectors and highlighted their thermal performance, very few publications have reported on the operation strategy, the optimum heat versus electricity storage, or evaluated the benefits under harsh weather conditions, such as extremely high ambient temperatures and high levels of aerosols prevalent in places like Saudi Arabia. The objective of this paper is to address these shortcomings using Saudi Arabia as a case study.

To do so, a detailed techno-economic theoretical assessment is carried out. A CPVT with a novel receiver design, suitable for the harsh conditions, is investigated under the climate of six cities in Saudi Arabia. To provide a comprehensive analysis, a mathematical model is developed to investigate the optical and thermal performance of the proposed CVPT. For each location studied, a year-round performance assessment considering the hourly variation of solar radiation, sun position, ambient temperature, and wind speed is conducted. A comparison is then made for all cities and under all operating and storage scenarios.

2. Materials and Methods

2.1. Description of the CPVT

A Linear Fresnel Collector (LFC) with a hybrid receiver fitted at its focal axis is proposed in this study. As illustrated in Figure 1, the proposed system consists of mirrors, a thermal receiver with cooling channel, a heat transfer fluid that also plays the role of a filter, and a silicon bifacial PV module with a 22% nominal efficiency at 25 °C. The mirrors focus direct normal irradiance on the receiver's front surface. The fluid is used as spectral filter, absorbing low and high-energy photons and converting them into useful heat. As a result, a suitable solar radiation spectrum for silicon PV cells reaches the PV module, which is placed above the nanofluid. Due to the bifaciality factor of the solar cell, the side with the highest efficiency faces the concentrated solar radiation to maximize energy production. The cooling channel is used to reduce the PV module temperature. The design values of the proposed system are presented in Table 1.

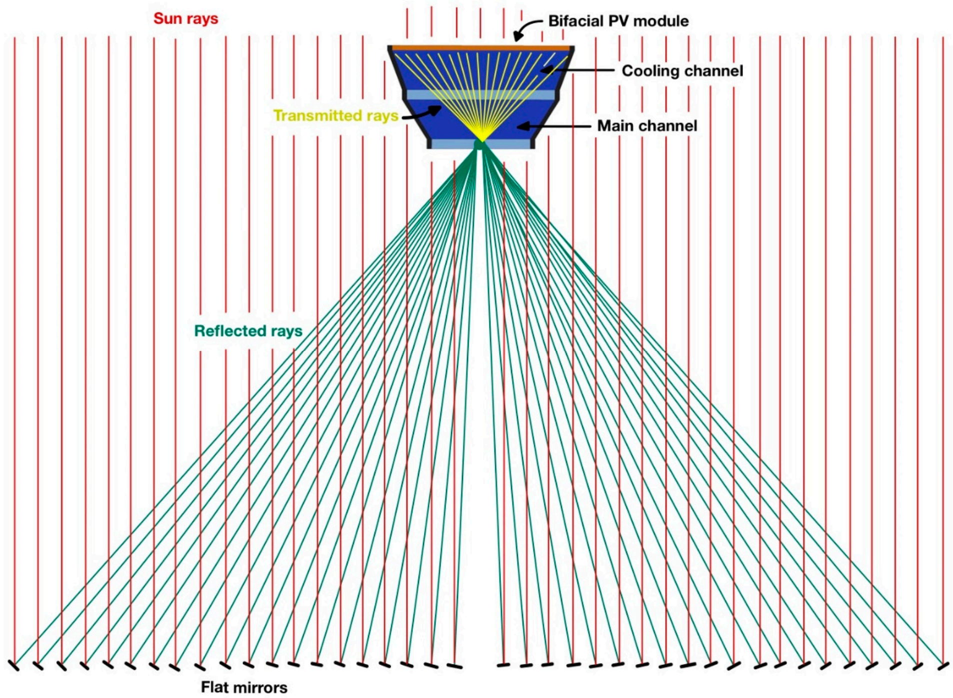

Figure 1. Basic design of the CPVT.

Table 1. Design data of the CPVT.

Component	Parameter	Value	Units
Linear Fresnel collector	Length	10	m
	Receiver focal length	1.5	m
Receiver	Height of the receiver	0.08	m
	Wide of the mirrors	0.1	m
	Wide of the receiver front surface	0.2	m
	Wide of the receiver back surface	0.33	m

A detailed design of the receiver is presented in Figure 2a. It consists of the main liquid channel and the cooling channel together with the PV module. As illustrated in Figure 2b, these two channels are linked by a U-shaped pipe to enhance thermal efficiency [22]. The liquid initially flows at room temperature through the cooling channel to cool down the PV panel. As a result, the panel's temperature drops, its efficiency increases, and the HTF is preheated before entering the main receiver channel. Figure 2c highlights the main parts of the receiver.

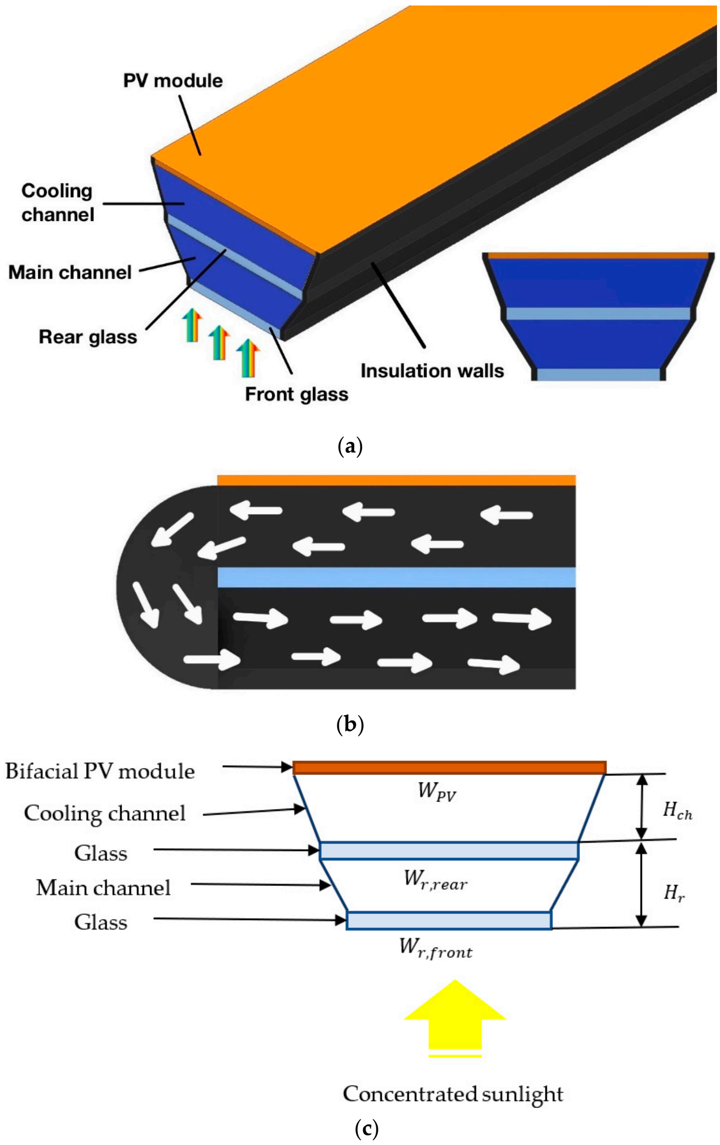

Figure 2. (**a**) CAD design of the receiver (cross-section). (**b**) U-shape pipe linking the cooling channel to the main channel. (**c**) Simplified design of the receiver.

As highlighted in Figure 2c, concentrated light passes through the highly transparent glass and across the working fluid. The working fluid acts as a spectral filter, absorbing solar radiation with wavelengths less than 700 nm or greater than 1100 nm. As a result, only solar radiation within the spectral window of between 700 nm and 1100 nm reaches the PV module. The receiver's side walls are painted with selective, highly absorbent materials.

In this study, two different working fluids, namely water and a water-based ZnO nanofluid (0.01 wt%), were examined. The introduction of nanoparticles into the water resulted in alterations within the thermophysical and spectral characteristics of the fluid, as documented in Tables 2 and 3, respectively. The evaluation of the thermophysical properties was carried out under atmospheric pressure and at an approximate average fluid temperature of 62.5 °C, representing an average working fluid temperature of our system.

Table 2. Thermo-physical properties of water and ZnO water-based nanofluid.

Symbol	Fluid Properties	Water	ZnO (0.01 wt%)
μ	Dynamic viscosity, mPas	0.47 [23]	0.47 *
k	Thermal conductivity, $Wm^{-1}K^{-1}$	0.65 [23]	0.86 [24]
Cp	Specific heat capacity, $Jkg^{-1}K^{-1}$	4185 [23]	4148 [25]
ρ	Density, kgm^{-3}	983.7 [23]	976.9 [25]

* Due to a lack of data, it is presumed that the dynamic viscosity does not change due to the low concentration of ZnO particles.

Table 3. Average spectral transmittance of water and ZnO water-based nanofluid for specific spectral windows.

Spectral Window	200–700 nm	700–1100 nm	1100–2400 nm
Water [2]	97.1	88.1	11.7
ZnO (0.01 wt%) [24]	64.3	79.8	5.1

The present investigation focuses on the photovoltaic active range of 700 nm to 1100 nm for silicon solar cells, in accordance with prior research [26]. Notably, the study does not encompass the photovoltaic active spectrum spanning 400–700 nm, where energy states surpass the bandgap energy of silicon, resulting in the thermal relaxation of excess photon energy. Nevertheless, the examined fluids exhibit a notable degree of radiation transmission within the 400–700 nm range, as demonstrated in Table 3, thus signifying their potential efficacy in capturing solar energy from this specific region.

2.2. Design of the CPVT

The CPVT collector is north–south orientated and rotates along the east–west horizontal axis to increase the overall optical performance and reduce variation in energy delivery during the day [27].

Three parameters are important in the design of the LFC (see Figure 3): location (M_n), tilt angle (δ_n), and distance of adjacent mirrors (S_n). These may be obtained using elementary geometrical optics by using the following formulas [28]:

$$\delta_n = \frac{\text{atan}\left(\frac{M_n}{fc_r}\right)}{2} \tag{1}$$

$$S_n = \frac{W_{mirror}}{2 \times \left[(\sin(\delta_n) + \sin(\delta_{n-1})) \times \tan(2\delta_n) + \cos(\delta_n) + \cos(\delta_{n-1})\right]} \tag{2}$$

$$M_n = M_{n-1} + S_n \tag{3}$$

where fc_r is the focal length of the receiver, W_{mirror} the width of the primary mirrors, and the subscript n is the number of the primary mirror.

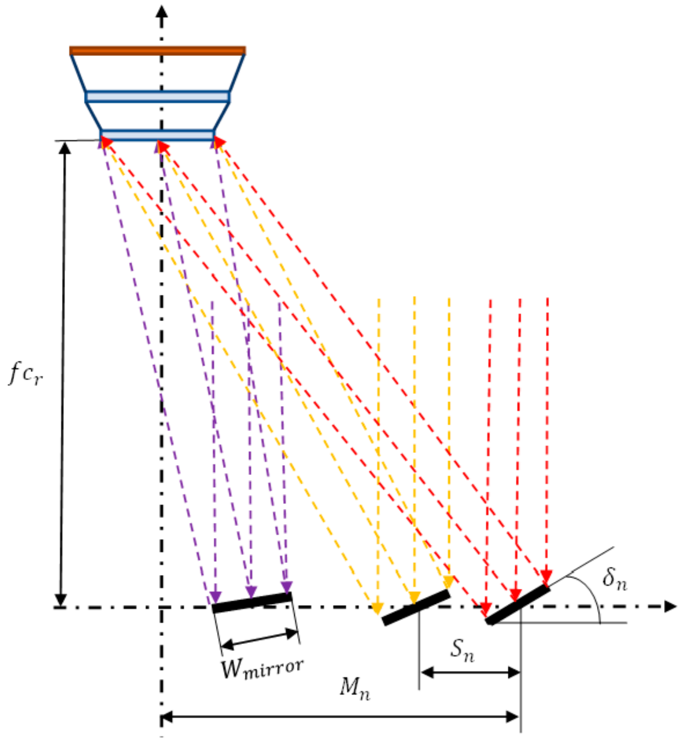

Figure 3. Schematic of the CPVT collector.

2.3. Optical and Thermal Modelling

2.3.1. Optical Efficiency

The following expression is used to estimate the optical efficiency of the LFC [29]:

$$\eta_{opt} = \eta_{opt,nom} K_T(\theta_T) K_L(\theta_L) \tag{4}$$

where $\eta_{opt,nom}$ is the nominal optical efficiency measured at solar noon, $K_T(\theta_T)$ is the transversal incidence angle modifier, θ_T is the transversal incidence angle in degree, $K_L(\theta_L)$ is the longitudinal incidence angle modifier, and θ_L is the longitudinal incidence angle in degree.

For a collector aligned along the north–south axis, the transversal and longitudinal angles are calculated as follows [27]:

$$\theta_T = \tan^{-1}(\sin(Az) \times \tan(Z)) \tag{5}$$

$$\theta_L = \tan^{-1}(\cos(Az) \times \tan(Z)) \tag{6}$$

where Az and Z are the Azimuth and Zenith angles, respectively.

In addition, the transversal and the longitudinal incidence angle modifiers are calculated using the following expressions, respectively [27]:

$$K_T(\theta_T) = \cos\left(\frac{\theta_T}{2}\right) - \frac{\frac{W_{field}}{4}}{fc_r + \sqrt{{fc_r}^2 + (\frac{W_{field}}{4})^2}} \times \sin(\frac{\theta_T}{2}) \tag{7}$$

$$K_L(\theta_L) = \cos(\theta_L) - \frac{fc_r}{L_r} \times \sqrt{1 + \left(\frac{W_{field}}{4fc_r}\right)^2} \times \sin(\theta_L) \tag{8}$$

where L_r is the receiver length, and W_{field} is the field width.

2.3.2. Heat Transfer Model

To examine the heat flow inside the receiver, a heat transfer model is developed. The flowchart outlining the model's structure and methodology can be found in Appendix A. The model takes into account the following set of assumptions:

- Steady state heat transfer model
- Thin PV module
- Side walls of the receiver are adiabatic
- Uniform temperature distribution
- The nanofluid flow is uniform

Furthermore, considering the phenomenon of self-absorption exhibited by the fluid and the similarity in emissivity between the fluid and the glass window, it is assumed that the heat radiation losses can be directly attributed to the glass window.

Heat Transfer in the Receiver

According to Newton's law of cooling, the convection heat transfer from the absorber's interior surface to the HTF is:

$$Q_{conv,r-fl} = h_{fl} \times A_{r,in} \times \left(T_{r,in} - T_{r,fl,mean}\right) \tag{9}$$

where $A_{r,in}$ is the inside surface of the thermal receiver, $T_{r,in}$ is the temperature of the inside surface of the thermal receiver, $T_{r,fl,mean}$ is the mean temperature of the fluid in the receiver, and h_{fl} is the fluid heat transfer coefficient defined in the following way:

$$h_{fl} = \frac{Nu_{fl} \times k_{fl}}{Dh_r} \tag{10}$$

where Nu_{fl} is the fluid Nusselt number, k_{fl} is the fluid thermal conductivity, and Dh_r is the hydraulic diameter of the receiver. For the case of laminar flow, the Nusselt number is considered constant:

$$Nu_{fl\_laminar} = 4.36 \tag{11}$$

For the case of turbulent flow, the following Nusselt number correlation is used:

$$Nu_{fl\_turbulent} = 0.023 \times {Re_{fl}}^{3/4} \times {Pr_{fl}}^{0.3} \tag{12}$$

where Re_{fl} is the Reynolds number and Pr_{fl} is the fluid Prandtl number.

Conduction through the front and rear glass of the receiver can be represented as follows:

$$Q_{cond,r} = \left(\frac{k_{glass} \times A_{r,glass} \times (T_{r,in} - T_{r,out})}{t_{glass}}\right) \tag{13}$$

where k_{glass} is the glass thermal conductivity, $A_{r,glass}$ is the area of the front and rear glass, $T_{r,out}$ is the temperature of the outside surface of the thermal receiver and t_{glass} the glass thickness.

The rear glass surface of the receiver is connected to the cooling channel, and the walls are insulated, so convective heat exchange with the ambient air is only considered on the front glass surface of the receiver. Consequently, following Newton's law of cooling, the convection heat transfer from the receiver's outside surface to the atmosphere is:

$$Q_{conv,r-amb} = h_{air} \times A_{r,out,front} \times (T_{r,out} - T_{amb}) \tag{14}$$

where $A_{r,out,front}$ is the front glass surface of the thermal receiver, T_{amb} is the ambient temperature during sun hours, and h_{air} is the air heat transfer coefficient defined in the following way:

$$h_{air} = \frac{Nu_{air} \times k_{air}}{Dh_r} \tag{15}$$

where Nu_{air} is the air Nusselt number, and k_{air} is the air thermal conductivity. For laminar flow over a flat plate, the Nusselt number is expressed as follows:

$$Nu_{air\_laminar} = 0.664 \times {Re_{air}}^{0.5} \times {Pr_{air}}^{1/3} \tag{16}$$

For turbulent flow over a flat plate, the Nusselt number is expressed as follows:

$$Nu_{air\_turbulent} = 0.037 \times {Re_{air}}^{0.8} \times {Pr_{air}}^{1/3} \tag{17}$$

Because the receiver's front glass surface is in contact with the ambient air and the sidewalls are insulated, convective heat exchange with the cooling channel is only evaluated on the receiver's rear glass surface. As a result, according to Newton's law of cooling, the convection heat transfer from the outer surface of the receiver to the cooling channel is:

$$Q_{conv,r-ch} = h_{fl} \times A_{r,out,rear} \times \left(T_{r,out} - T_{ch,fl,mean}\right) \tag{18}$$

where $A_{r,in}$ is the inside surface of the thermal receiver, $T_{r,in}$ is the temperature of the inside surface of the thermal receiver, $T_{ch,fl,mean}$ is the mean temperature of the fluid in the cooling channel and h_{fl} the fluid heat transfer coefficient.

According to the Stefan–Boltzmann law of radiation, the radiation heat transfer from the external surface of the receiver to the atmosphere is:

$$Q_{rad,r-atm} = \sigma \times \varepsilon_{glass} \times A_{r,out,front} \times \left({T_{r,out}}^4 - {T_{sky}}^4\right) \tag{19}$$

where σ is the Stefan-Boltzmann constant $\left(5.67 \times 10^{-8}\ \mathrm{Wm^{-2}K^{-4}}\right)$, ε_{glass} is the glass emissivity, and T_{sky} is the sky temperature estimated using the following expression [30]:

$$T_{sky} = 0.0522 \times {T_{amb}}^{1.5} \tag{20}$$

Radiation heat exchange with the PV panel is only evaluated on the receiver's rear glass surface. As a result, the expression that estimates the radiation heat transfer between two parallel plates is used:

$$Q_{rad,r-PV} = \left(\frac{\sigma \times A_{r,out,rear} \times \left({T_{r,out}}^4 - {T_{PV}}^4\right)}{\frac{1}{\varepsilon_{glass}} + \frac{1}{\varepsilon_{PV}} - 1}\right) \tag{21}$$

where T_{PV} is the temperature of the PV panel, and ε_{PV} is its emissivity.

Heat Transfer in the PV Panel

The solar radiation on the rear surface of PV cell follows the Stefan–Boltzmann law of radiation:

$$Q_{rad,PV-atm} = \sigma \times \varepsilon_{PV} \times A_{PV,rear} \times ({T_{PV}}^4 - {T_{sky}}^4) \tag{22}$$

where $A_{PV,rear}$ is the area of the PV panel rear surface.

Newton's law of cooling states that the convective heat transfer from the PV panel to the cooling channel is:

$$Q_{conv,PV-ch} = h_{fl} \times A_{PV,front} \times (T_{PV} - T_{ch,fl,mean}) \tag{23}$$

where $A_{PV,front}$ is the front surface of the PV panel, and h_{fl} is the fluid heat transfer coefficient.

The convective heat transfer from the PV panel to the ambient air is:

$$Q_{conv,PV-amb} = h_{air} \times A_{PV,rear} \times (T_{PV} - T_{amb}) \tag{24}$$

where h_{air} is the air heat transfer coefficient.

Power, Efficiency and Energy

The efficiency of bifacial crystalline silicon PV cells can be estimated using the following expression, which considers a temperature coefficient of $-0.45\%/°C$:

$$\eta_{PV} = \eta_{PV,nom}[1 - (0.0045 \times (T_{PV} - T_{PV,ref}))] \quad (25)$$

where $\eta_{PV,nom}$ is the nominal efficiency of the PV panel at the reference temperature $T_{PV,ref}$. The electric energy produced by the PV panel can be calculated using the following equation:

$$Q_{u,PV,el} = DNI \times A_{ap} \times \eta_{opt} \times \left(1 - f_{opt}\right) \times tr_{fl,700-1100nm} \times \eta_{PV} + GHI \times A_{PV,rear} \times \eta_{PV} \quad (26)$$

where DNI is the direct normal irradiance, f_{opt} is the fraction of optical loss in the receiver, $tr_{fl,700-1100\text{nm}}$ is the average spectral transmittance of the fluid filter between the 700–1100 nm spectral window, A_{ap} is the aperture area of the primary mirrors, and GHI is the global horizontal irradiance.

The power absorbed by the receiver is calculated using the following equation:

$$Q_{abs,r} = DNI \times A_{ap} \times \eta_{opt} \times f_r \quad (27)$$

where f_r is the fraction of radiation absorbed by the receiver.

The useful thermal power absorbed by the fluid in the receiver is:

$$Q_{u,fl,th,r} = \dot{m}_{fl} \times Cp_{fl} \times (T_{r,fl,out} - T_{ch,fl,in}) \quad (28)$$

where Cp_{fl} is the specific heat capacity of the fluid, $\dot{m}_{fl}$ is the fluid mass flow rate, $T_{r,fl,out}$ is the temperature of the fluid in the outlet of the receiver, and $T_{ch,fl,in}$ is the temperature of the fluid in the inlet of the cooling channel. As a result, the thermal efficiency of the receiver may be calculated as follows:

$$\eta_r = \frac{Q_{u,fl,th,r}}{Q_{abs,r}} \quad (29)$$

The organic Rankine cycle (ORC) has received a great deal of attention as a well-accepted technology because it can make effective use of low-grade thermal energy sources, such as solar thermal [31]. In the present study, one of the scenarios examined considers that the thermal energy stored in the fluid is converted to electrical energy through an ORC. Therefore, the overall electrical efficiency of the system is defined as follows:

$$\eta_{total,el} = \eta_{PV} + [\eta_r \times \eta_{heat-Carnot} \times \left(1 - \frac{T_{amb}}{T_{r,fl,out}}\right)] \quad (30)$$

where $\eta_{heat-Carnot}$ is the thermodynamic efficiency of heat engine to Carnot efficiency [32].

Lastly, the net solar-to-electric efficiency of the system, which incorporates the total incident solar power as a common denominator, is presented as:

$$\eta_{NSE} = \frac{Q_{u,PV,el} + Q_{u,fl,th,r} \times \eta_{heat-Carnot} \times \left(1 - \frac{T_{amb}}{T_{r,fl,out}}\right)}{\text{DNI} \times A_{ap}} \quad (31)$$

3. Results and Discussion

3.1. Ray Tracing and Optimum Geometric Concentration Ratio of the CPVT

A ray-tracing simulation of the LFC has been carried out using Tonatiuh software to assess the design of the proposed CPVT (see Figure 4). Figure 5 illustrates the heat flux distribution on the front glass of the receiver. As can be noticed, the flux distribution corresponds to that of a typical LFC.

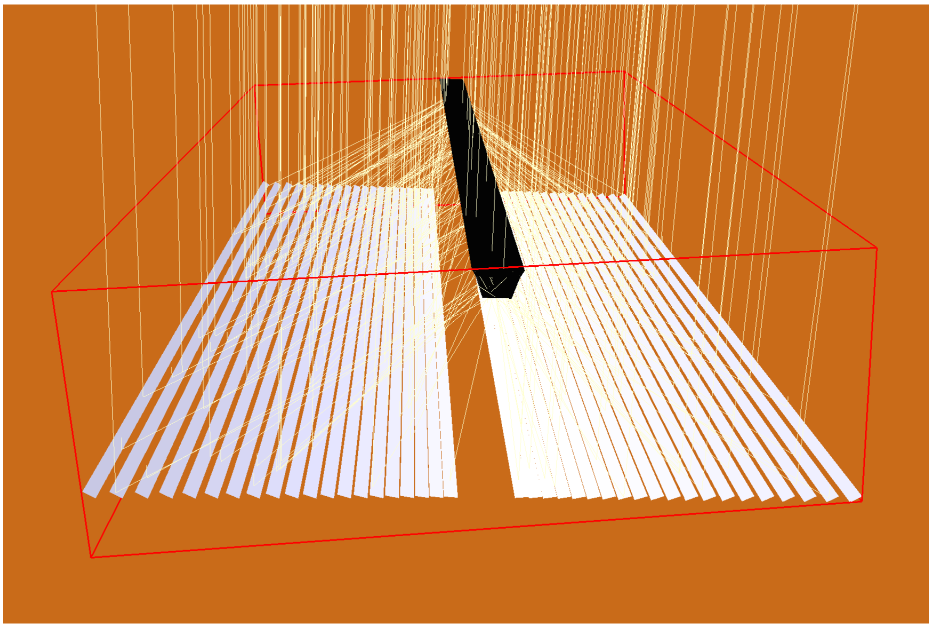

Figure 4. Ray tracing simulation with 250 rays using Tonatiuh software.

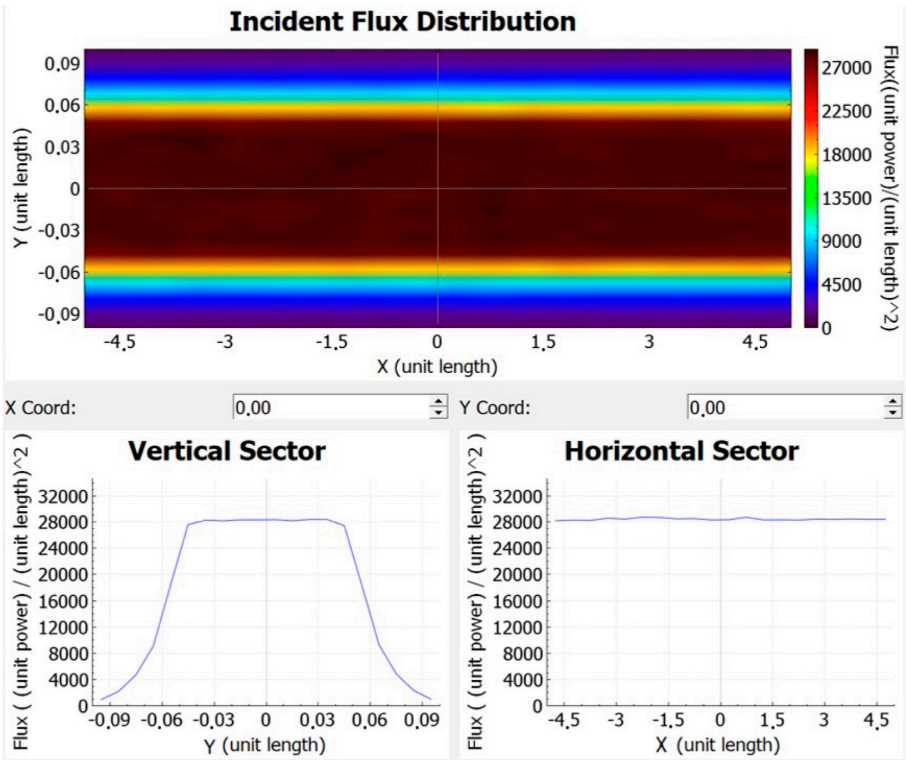

Figure 5. Front glass of the receiver flux distribution, simulation with 1x10^7 rays using Tonatiuh software.

A parametric study is carried out to determine the optimum concentration ratio for the CPVT collector. Average weather data for Tabuk was employed for this optimization process. Figure 6 illustrates the variation of the overall electric efficiency and the temperature of the PV module as a function of the geometric concentration ratio (GCR) of the CPVT collector. As can be seen, the optimum GCR that maximize the overall electric efficiency of the CPVT collector is about 20. At this GCR, the temperature of the PV module is less than 85 degree C (the maximum operating temperature of crystallin PV cells). Therefore, this value is used in this study.

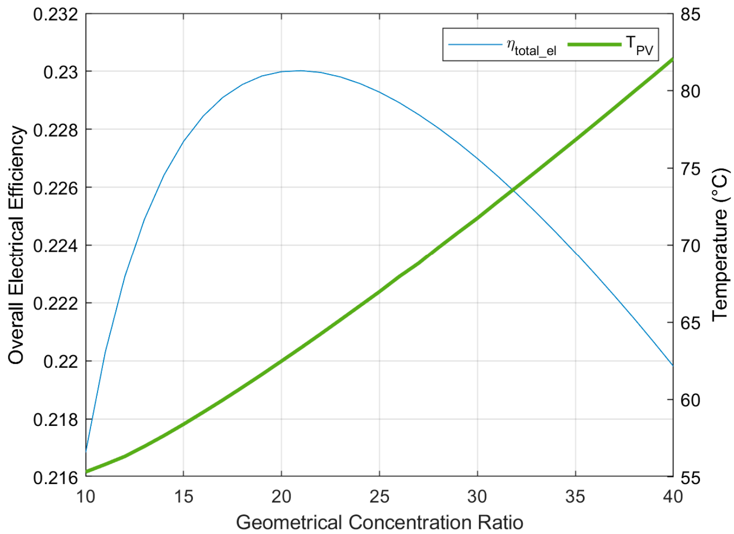

Figure 6. Optimum geometric concentration of the CPVT collector.

3.2. Advantages of the Proposed Receiver Design

To highlight the advantages of the proposed receiver design, an annual performance comparison between a receiver with cooling the PV module (denoted C in this paper) and a receiver without cooling the PV module (denoted NC in this paper) has been conducted. Six different locations and two different HTFs—water (denoted W in this paper) and water with ZnO nanoparticles at 0.01 wt% concentration (denoted W+ZnO in this paper)—are considered.

As can be noticed in Figure 7, the average temperature of the PV module is lower for the case with cooling than for the case without cooling (more than 10 °C difference). This results in higher efficiency of the PV cells. The addition of ZnO nanoparticles to water improves the heat transfer, which further reduces the temperature of the PV module; thus, high electric efficiency is achieved.

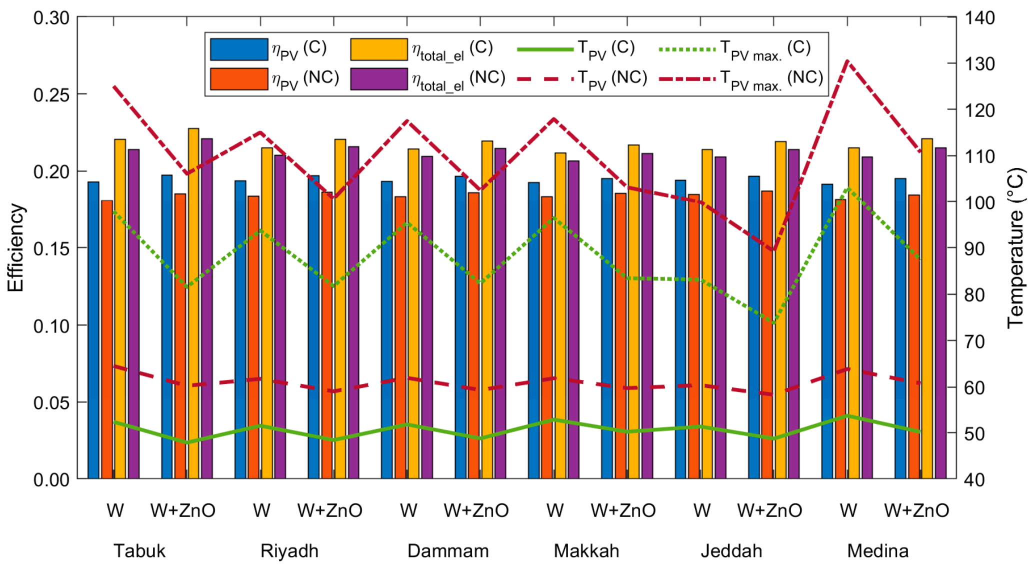

Figure 7. Annual average values of PV module efficiency (η_{PV}), total efficiency of CPVT collector ($\boldsymbol{\eta_{total,el}}$), temperature of PV module (T_{PV}), and maximum temperature of PV module.

Overall, the performance of the CPVT collector at Tabuk is better than other locations because of the low ambient temperature and the high solar irradiance (see Table 4).

Table 4. Annual average values of direct normal irradiance (DNI), global horizontal irradiance (GHI), ambient temperature, wind speed, and optical efficiency of CPVT collector (η_{opt}).

Location	*DNI* (W m^{-2})	*GHI* (W m^{-2})	T_{amb} (°C)	V_{wind} (ms^{-1})	η_{opt} (%)
Tabuk	599	524	27.2	3.5	54.2
Riyadh	452	501	30.6	3.7	55.3
Dammam	441	494	31.1	3.6	55.3
Makkah	427	487	34.6	4.4	55.0
Jeddah	426	493	32.8	4.4	54.9
Medina	516	512	32.5	4.1	54.8

3.3. Thermal Performance of the CPVT

The yearly energy production of the CPVT at different locations is illustrated in Figure 8. The PV electrical energy output and thermal energy output are higher when the CPVT is installed in Tabuk. When ZnO nanoparticles are added to water, the thermal energy increases in all the considered locations, but the electrical energy provided by the PV panel slightly decreases. Although the drop in electrical energy is small compared to the gain in thermal energy, if all the thermal energy is converted to electricity, less energy is obtained compared with the case of using water.

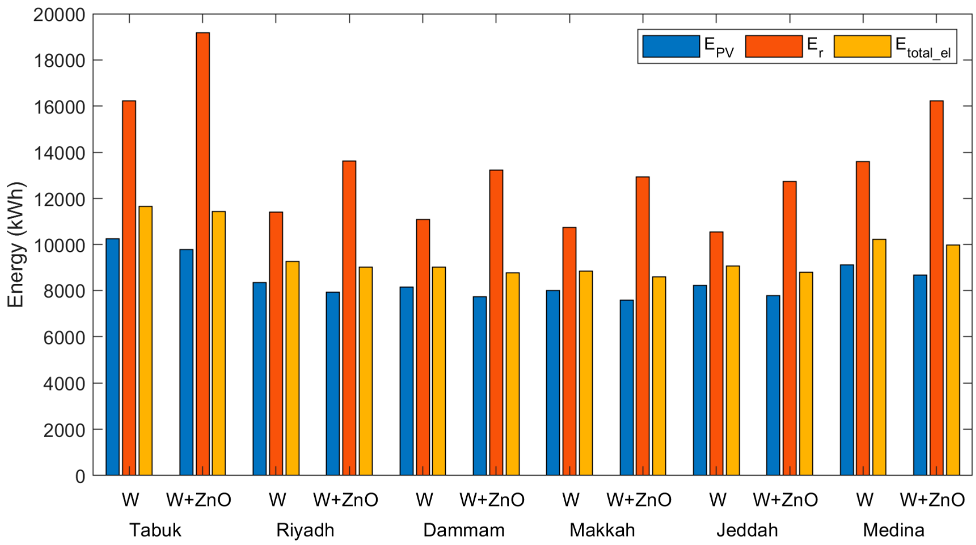

Figure 8. Annual energy production of the CPVT system.

The monthly energy production in Tabuk is shown in Figure 9. Summer months always have the highest energy output. The amount of energy produced varies dramatically throughout the year, with the summer period producing twice as much electrical energy and up to four times more thermal energy compared to winter months. This is because solar radiation is higher in the summer than in the winter, and the optical efficiency of the system is also higher.

Figure 9 also highlights that, when ZnO nanoparticles are added to water, the thermal energy output increases. This is because the working fluid absorbs 6.2% more solar radiation, as shown in Table 5, due to the variation in the spectral transmittance property, when ZnO is added to the water. On the other hand, when the working fluid contains nanoparticles, the electrical production is slightly lower. The scientific reason behind it is that the nanofluid absorbs more solar radiation at wavelengths between 700 nm and 1100 nm; these wavelengths are used to generate energy through the photovoltaic effect for silicon-based PV panels. In this spectral window, water alone has an average spectral transmittance of 88.1% [2], which drops to 79.8% [24] when ZnO nanoparticles are added.

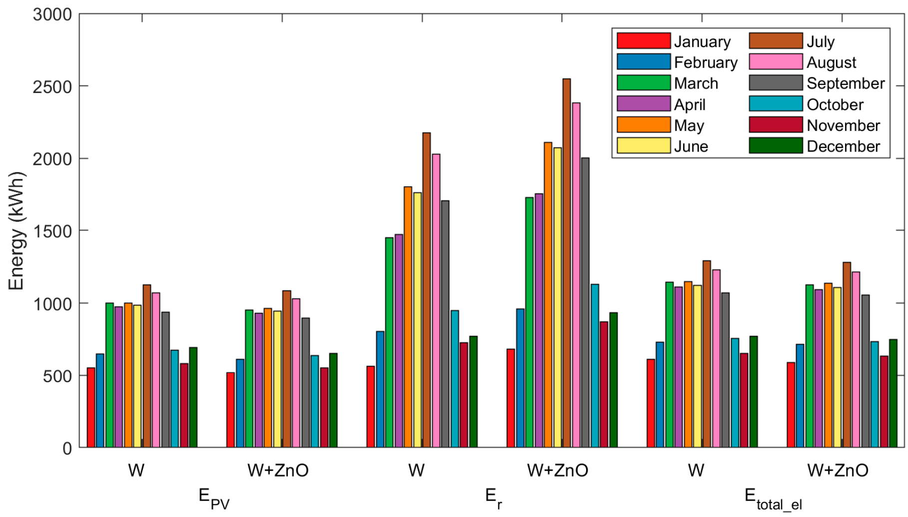

Figure 9. Energy production per month in Tabuk.

Table 5. Percentage of light power absorbed by component using different fluid filters.

Fluid Filter	PV Module (%)	Fluid (%)	Receiver Walls (%)	Thermal Unit (%)	Optical Loss (%)
Water [2]	31.5	23.1	33.2	56.3	12.2
Water-ZnO	25.3	29.3	33.2	62.5	12.2

Values for water-ZnO nanofluid calculated using the spectral transmittance presented by Huaxu et al. [33] at 0.01 wt% concentration.

A monthly analysis of the efficiency for the PV panel and the receiver in Tabuk is illustrated in Figure 10. It is notable that the variation in the efficiency for the PV panel is not significant during the year. The PV efficiency is slightly better in the winter period compared to the summer period due to lower ambient temperature. In contrast, the net solar-to-electric and thermal receiver efficiencies follow the same trend as thermal energy generation, being higher in summer than in winter.

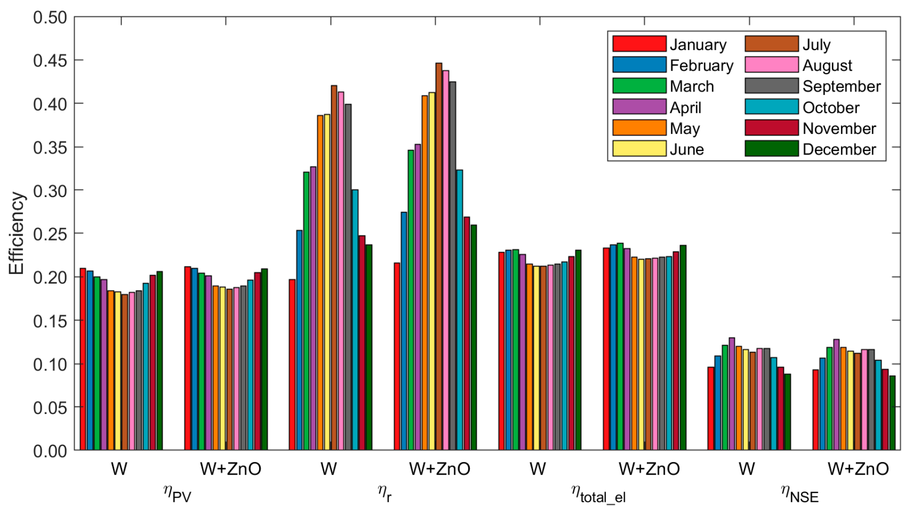

Figure 10. Energy efficiency per month in Tabuk.

3.4. Economic Analysis

3.4.1. CAPEX of the CPVT

The estimation of the cost of the CPVT is based on the Hyperlight Energy project. Table 6 highlights the specific costs as well as the total CAPEX of the CPVT collector considered in this study [34,35]. The cost of bifacial photovoltaic panels has been evaluated based on an average of projects completed in the last few years following the IRENA report [36]. Estimation showed that the CPVT collector with nano-particles costs $8550, while a CPVT collector with water as a HTF costs $200 less.

Table 6. CAPEX of a CPVT collector.

Component	Value	Unit	Cost ($)
Site improvement	5 [34]	$/m^{2}mirror	200
Primary mirrors	110 [34]	$/m^{2}mirror	4400
Thermal receiver (HTF, piping, etc.)	60 [34]	$/m^{2}mirror	2400
Bifacial crystalline silicon cells (Total ins.)	1.5 [36]	$/Wp	1350
ZnO 0.01 wt% (preparation, product)	5 [37]	$/m^{2}mirror	200
TOTAL CPVT COST			8550

3.4.2. The LCOE and LCOH for a 20 MW CPVT Plant

The LCOE and LCOH represent the average of the net present cost of energy production for the plant over its lifetime. The IRENA methodology is used in this paper [36]:

$$LCOE\ or\ LCOH = \frac{\sum_{t=1}^{n} \frac{I_t + OM_t}{(1+r)^t}}{\sum_{t=1}^{n} \frac{E_t}{(1+r)^t}} \tag{32}$$

where I_t are the investment expenditures in the year t, OM_t are the operations and maintenance expenditures in the year t, E_t is the energy generation in the year t, r is the discount rate, and n is the lifetime of the system.

The financial parameters that were used by IRENA are adapted in this study. These include: a 10% discount rate, a lifetime of 25 years, and 3% of the CAPEX were considered for the maintenance and operation costs.

Two operation strategies are considered, namely electricity production strategy and heat/electricity production strategy. In the former, the heat absorbed by the HTF is converted into electricity using an ORC cycle. The electricity may either be fed directly into the power grid or used to power an industry or households in remote places. A 20 MWh thermal energy storage (TES) consisting of a water tank is considered to store thermal energy with 82% round-trip-efficiency. In a heat/electricity production strategy, it is assumed that there is an industry nearby requiring hot water at 95 °C. This is highly feasible given that the industrial sector with low-temperature heat processes accounts for 7.1% of world energy consumption [38].

To calculate the LCOH and the LCOE of a large-scale CVPT power plant, it is important to estimate the CAPEX. Considering that the LFC uses an average of 70% of the total land, the cost of the land required was estimated at $5/m^2. The cost of a TES system with a capacity of 20,000 kWh has been evaluated taking data from the European Association of Storage of Energy [39], and adding an extra cost of 15$/kWh for each system owing to the cost of building work and additional materials, like pipes. For the situation when the thermal energy is converted into electricity, the cost of the plant required has been determined using a Pratt and Whitney ORC catalogue [40]. Project efforts have also been considered and are estimated at 22.5% of the total cost of the solar plant.

Finally, an additional 5% has been added to the overall expenditures to compensate for any unanticipated occurrences throughout the project's execution phase. The sum of all the expenditures is the capital expenditure (CAPEX), which is given in Tables 7 and 8 for both operation strategies.

Table 7. CAPEX for electricity production strategy, 20 MW CPVT plant with water + ZnO installed in Tabuk.

Component	Value	Unit	Cost ($)	
Design Type			**NC**	**C**
CPVT system	8550	$/system	5,985,000	
Land costs (60,060 m^2)	5	$/m^2$	300,300	
Water storage system (20,000 kWh)	30 [39]	$/kWh	600,000	
Power plant unit (all included)	2400 [40]	$/kW	4,451,089	3,966,506
Project efforts (22.5% of solar plant costs)	22.5%	N/A	2,550,687	2,441,656
Uncertainties (5% of total costs)	5%	N/A	694,353.8	664,673
CAPEX			14,581,431	13,958,136

Table 8. CAPEX for electricity + heat production strategy, 20 MW CPVT plant with water + ZnO installed in Tabuk.

Component	Value	Unit	Cost ($)	
Design Type			**NC**	**C**
CPVT system	8550	$/system	5,985,000	
Land costs (60,060 m^2)	5	$/m^2$	300,300	
Water storage system (20,000 kWh)	30 [39]	$/kWh	600,000	
Project efforts (22.5% of solar plant costs)	22.5%	N/A	1,549,192	
Uncertainties (5% of total costs)	5%	N/A	421,724	
CAPEX			8,856,217	

Table 9 illustrates the values of the LCOE, LCOH, and CAPEX in different locations. Overall, the LCOE is lower for the proposed design (C) compared with the traditional design (NC). This proves the advantages of using the novel design proposed in this study. The addition of ZnO nanoparticles to the water increases the LCOE but decreases the LCOH.

An important finding of this study is that the heat/electricity production strategy is much better than the electricity production strategy. For instance, at Tabuk, the LCOE for our proposed design with water as HTF is 0.2232 USD/kWh when the electricity production strategy is selected. However, it is only 0.0847 USD/kWh when heat/electricity production is selected. Indeed, the LCOE when the heat/electricity production strategy is selected is lower than that of CSP (and the heat is produced as a by-product for free).

The most suitable location for installing CPVT technology in Saudi Arabia is at Tabuk. The analysis shows a LCOE of $0.0847/kWh and a LCOH of $0.0536/kWh when water is used as a spectral filter, and a LCOE of $0.0906/kWh and a LCOH of $0.0462/kWh when ZnO nanoparticles are added.

The LCOE of CPVT systems has been investigated in a limited number of scientific papers. In this study, we compare our results with some previously published studies, as shown in Table 10. Some of these studies have used PTC, which is more expensive than the technology of LFC used in our proposed design. Additionally, Fernandez et al. [41] have employed more expensive materials, such as ITO nanocrystals and Au nanoparticles, instead of the ZnO nanoparticles used in our system. Furthermore, Ling et al. [10] have used a solid oxide fuel cell (SOFC) instead of an ORC to transform electrical energy into thermal energy, which requires the purchase of methanol, implying additional expenses. Moreover, according to the NREL database [42], the DNI and GHI in Shiraz are 7% and 10% lower, respectively, compared to Tabuk. Taking into account these differences and the novelty of our design for harsh environments, the proposed CPVT system offers a lower LCOE, making it a more cost-effective solution for the given geographical area.

Table 9. LCOE, LCOH, and CAPEX of the CPVT power plants for different scenarios. Note, system with cooling is denoted as C and without cooling as NC.

Location	Scenario	Fluid Filter	LCOE ($/kWh)		LCOH ($/kWh)		CAPEX ($)	
	Design Type		NC	C	NC	C	NC	C
Tabuk	All electricity	Water	0.2451	0.2232			13,533,991	12,985,307
		Water+ZnO	0.2670	0.2442			14,581,431	13,958,136
	Electricity + heat	Water	0.0916	0.0847	0.0479	0.0536	8,676,142	8,676,142
		Water+ZnO	0.0977	0.0906	0.0416	0.0462	8,856,217	8,856,217
Riyadh	All electricity	Water	0.2697	0.2495			11,993,164	11,555,130
		Water+ZnO	0.2942	0.2727			12,803,027	12,298,728
	Electricity + heat	Water	0.1109	0.1042	0.0669	0.0762	8,676,142	8,676,142
		Water+ZnO	0.1193	0.1120	0.0574	0.0651	8,856,217	8,856,217
Dammam	All electricity	Water	0.2742	0.2539			11,878,377	11,448,747
		Water+ZnO	0.2988	0.2771			12,663,564	12,168,329
	Electricity + heat	Water	0.1138	0.1068	0.0687	0.0784	8,676,142	8,676,142
		Water+ZnO	0.1223	0.1148	0.0590	0.0670	8,856,217	8,856,217
Makkah	All electricity	Water	0.2719	0.2552			11,540,492	11,275,797
		Water+ZnO	0.2976	0.2794			12,301,948	11,985,618
	Electricity + heat	Water	0.1147	0.1085	0.0736	0.0808	8,676,142	8,676,142
		Water+ZnO	0.1238	0.1170	0.0625	0.0685	8,856,217	8,856,217
Jeddah	All electricity	Water	0.2666	0.2500			11,647,527	11,338,953
		Water+ZnO	0.2927	0.2744			12,439,096	12,074,460
	Electricity + heat	Water	0.1116	0.1057	0.0741	0.0824	8,676,142	8,676,142
		Water+ZnO	0.1207	0.1142	0.0627	0.0696	8,856,217	8,856,217
Medina	All electricity	Water	0.2542	0.2359			12,401,737	12,058,328
		Water+ZnO	0.2779	0.2585			13,295,356	12,895,731
	Electricity + heat	Water	0.1014	0.0951	0.0583	0.0638	8,676,142	8,676,142
		Water+ZnO	0.1089	0.1021	0.0500	0.0546	8,856,217	8,856,217

Table 10. Comparison of the LCOE.

References	Location	Technology	LCOE ($/kWh)
Ling et al. [10]	Not available	LFC with solid filter	0.2000
Rodrigeus et al. [41]	Blythe, California	PTC with nanofluid filter	0.1783
Abedanzadeh et al. [43]	Shiraz, Iran	PTC with pieces of mirrors	0.1293
Present study	Tabuk, Saudi Arabia	LFC with fluid filter	0.0847
Present study	Tabuk, Saudi Arabia	LFC with nanofluid filter	0.0906

3.4.3. CO_2 Emission Analysis

According to the Brown to Green 2019 report, the national emissions in Saudi Arabia associated with electricity generation in 2019 were 0.723 kgCO_2-equivalent for each kWh produced [44]. Moreover, according to the Ministry of Spain, emissions from stationary combustion equipment powered by natural gas (such as boilers) are 0.209 kgCO_2-equivalent per kWh generated [45]. These two variables are used as the electricity and thermal emissions factors, respectively, to compute, based on the energy production, the emission savings due to the use of CPVT technology. Figures 11 and 12 show the results for one single CPVT collector and for a 20 MW CPVT plant, respectively.

The implementation of the proposed CPVT can cut off annual emissions by 11.2 tCO_2eq (Tabuk) per system and from 5675 tCO_2eq (Makkah) to 7822 tCO_2eq (Tabuk) per 20 MW plant if the heat/electricity production strategy is selected. However, if the electricity production strategy is selected, this technology can save a total of 8.5 tCO_2eq per collector and 5968 tCO_2eq per 20 MW CPVT plant annually.

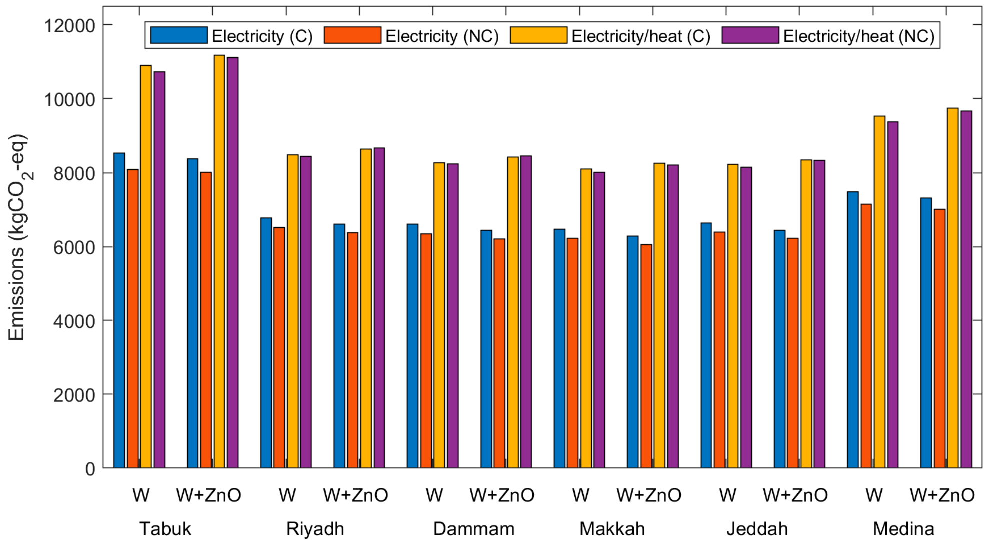

Figure 11. kgCO_2-equivalent emissions saved in KSA with one CPVT system.

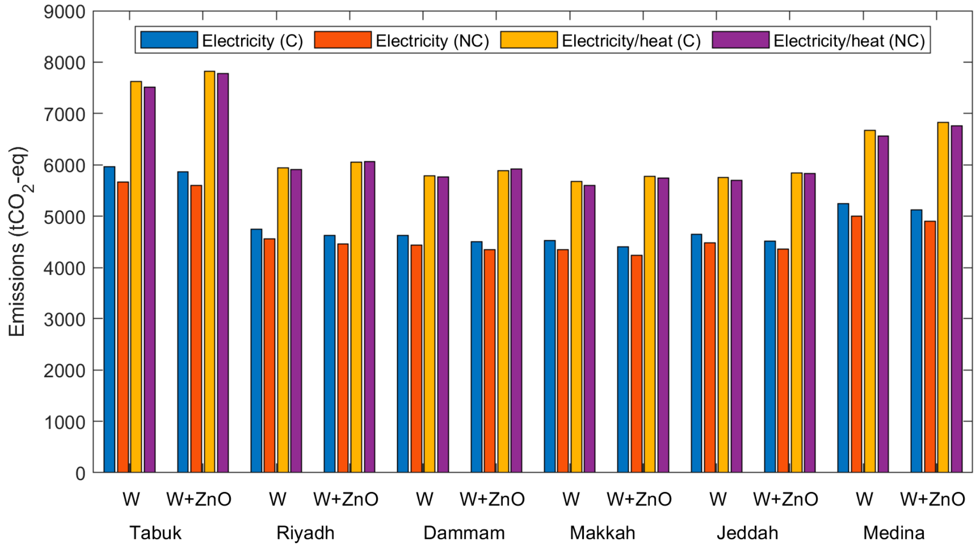

Figure 12. tCO_2-equivalent emissions saved in KSA with a 20 MW plant.

3.4.4. Battery vs. TES

A large increase in battery production is expected in the coming years. However, the materials needed for their production are limited, so it is critical to look for other ways of storing energy. For this reason, a thermal energy storage (TES) system has been considered in this study, and its comparison in economic terms is shown below.

The cost of lithium-ion battery packs has increased for the first time since 2010 because of rising inflation and prices of raw materials and battery components, reaching an average of 151$/kWh in 2022 [46]. Moreover, in the most optimistic scenario, lithium-ion batteries have a lifetime of 15 years, so they would have to be replaced at least once to match the lifespan of the solar power system [47,48]. On the other hand, according to the European Association for Energy Storage, the price for a hot water storage tank is 15$/kWh with an average 30-year working life.

For the battery scenario, the heat is first converted to electricity using an ORC with an efficiency on the order of 10% for the working temperatures considered in this study (see Equation (30)). Afterwards, electricity is stored into a 20 MWh lithium-ion battery which nowadays reach up DC round-trip efficiency values as high as 95% [49]. Alternatively, the MWh TES system with 82% round-trip efficiency previously described in Section 3.4.2 can be used, with no need to convert the heat into electricity for storage. Table 11 compares the two suggested storage systems installed in Tabuk based on the LCOE, LCOH, and CAPEX for a 20 MW large-scale plant, in which an extra cost of 15$/kWh has been estimated for each system owing to the cost of building work and additional materials like cables or pipes.

Table 11. LCOE, LCOH, and CAPEX of the CPVT with cooling for different energy storage types in Tabuk.

Location	Scenario	Fluid Filter	LCOE ($/kWh)		LCOH ($/kWh)		CAPEX ($)	
	Storage Type		TES	Battery	TES	Battery	TES	Battery
Tabuk	All electricity	Water	0.2232	0.3502			12,985,307	20,368,382
		Water+ZnO	0.2442	0.3734			13,958,136	21,341,211
	Electricity + heat	Water	0.0847	0.1568	0.0536	0.0991	8,676,142	16,059,217
		Water+ZnO	0.0906	0.1661	0.0462	0.0848	8,856,217	16,239,292

The use of batteries compared to a TES system based on a water tank represents an additional increase of 5.74 million dollars, considering that the batteries will need to be replaced once during the lifetime of the solar plant. This represents an even greater increase in the CAPEX, which is reflected in the LCOE and LCOH costs, which increase up to 56% and 84% respectively.

3.5. Future Work

In terms of future work, there are several areas of research that could be explored to further enhance the performance of concentrated photovoltaic-thermal (CPVT) systems. Building a prototype to experimentally validate the theoretical outcomes of this study would be a valuable next step. This would provide a more accurate representation of the real-world performance of the CPVT system.

Another possible avenue of research would be to include the capability of joining multiple CPVT systems in series in the mathematical model presented. This would allow for a higher heat transfer fluid output temperature, expanding the range of potential applications beyond just low-temperature heating.

Furthermore, it may be useful to explore the recommendations of An et al. [50] and investigate the effectiveness of using two reflectors at the sides of the solar receiver to minimize the effect of imprecise sun tracking and receiver installation. This could potentially reduce the current optical losses of the proposed solar receiver (12.2%) and improve the overall performance of the CPVT system.

Overall, this study contributes to the body of knowledge on CPVT systems and provides valuable insights for future research in this area. There is still much to be explored in terms of optimizing the performance and applicability of CPVT systems, and the proposed future research directions could help to advance this field.

4. Conclusions

The design and performance evaluation of a novel CPVT with spectral beam splitting technology, a cooling channel, and nanofluid is presented in this paper. A raytracing simulation tool is used to assess optical performance of the proposed CPVT collector, while an optical-thermal model is used to estimate the performance of the system.

The investigation revealed that using fluids as a filter in the CPVT collector has numerous benefits, including a low operating temperature for the PV cells and a high energy output. By adding the cooling channel and ZnO nanoparticles, it is found that a significant decrease in the average and maximum temperature of the PV panel is achieved, where they are lowered by 16.6 °C and 43.4 °C, respectively. This allows conventional silicon photovoltaic panels which have a maximum operating temperature of 85 °C [51] to be used. Therefore, without these design improvements, we would have to resort to special high-temperature PV panels, which are in very limited supply from manufacturers and present lower efficiencies due to the increased temperature.

The calculated yearly average values of the efficiencies, with the addition of the cooling channel and nanofluid, are, for Tabuk, 19.74% for the photovoltaic panel, 35.65% for the thermal collector, and 22.65% for the total conversion to electricity.

The economic assessment showed that the CPVT system has great possibilities to lead the Saudi renewable energy production in the coming years. Under a heat/electricity production strategy, a LCOE of $0.0847/kWh and a LCOH of $0.0536/kWh when only water is used a HTF are obtained. At the same time, a LCOE of $0.0906/kWh and a LCOH of $0.0462/kWh are obtained when ZnO particles are added. The analysis showed that, due to the low performance and high costs of converting thermal energy into electricity, the CPVT technology is less competitive when the electricity production strategy is selected. The results showed an LCOE of $0.2232/kWh with water only and $0.2442/kWh with the addition of ZnO nanoparticles.

Furthermore, after comparing battery energy storage against a TES system, a large increase in the CAPEX was observed if batteries are used, reflected in the LCOE and LCOH costs, which increase up to 56% and 84% (compared with the case of TES), respectively. Thus, a CPVT plant with TES operating under a heat/electricity production strategy is better than a CPVT plant with battery operating under an electricity production strategy.

The study showed that a 20 MW CPVT plant cuts CO_2-equivalent emissions up to 7822 tonnes every year under Saudi Arabian conditions. Another benefit in terms of sustainability is the ease of recycling the proposed CPVT technology, taking up less space, and requiring less photovoltaic material to capture the same sunlight as non-concentrating PV modules. Thus, the process is less dependent on the silicon supply chain.

Regarding the practicality of the technology presented, it has been demonstrated that the system is technically feasible through a series of rigorous computations and simulations. Specifically, the results indicate that the proposed design offers significant advantages when operating in harsh environments when compared to traditional designs. Additionally, an economic study was conducted which revealed that the system can be constructed at a relatively low cost in comparison to previous publications, resulting in an improved levelized cost of energy (LCOE) for this technology. Overall, these findings support the practicability of the technology, and suggest that it has the potential to be a viable cost-effective solution for a range of real-world energy applications.

Author Contributions: Conceptualization, C.L., O.B. and B.D.; Methodology, C.L., O.B. and B.D.; Software, C.L. and O.B.; Formal analysis, C.L.; Investigation, C.L., O.B. and B.D.; Resources, B.D.; Writing—original draft, C.L.; Writing—review & editing, O.B. and B.D.; Visualization, C.L.; Supervision, O.B. and B.D.; Project administration, B.D.; Funding acquisition, B.D. All authors have read and agreed to the published version of the manuscript.

Funding: Project is supported by Prof Bassam Dally KAUST baseline fund.

Data Availability Statement: Not applicable.

Acknowledgments: The authors gratefully acknowledge the funding of the King Abdullah University of Science and Technology.

Conflicts of Interest: The authors declare no conflict of interest.

Nomenclature

Abbreviations:

PV	Photovoltaic
CPVT	Concentrating solar photovoltaic thermal
LCOE	Levelized cost of electricity
LCOH	Levelized cost of heat
SBS	Spectrum beam splitting
HTF	Heat transfer fluid

PTC	Parabolic trough collector
LFC	Linear Fresnel collector
TE	Thermoelectric generator
NREL	National Renewable Energy Laboratory
DNI	Direct normal irradiance
GHI	Global horizontal irradiance
ORC	Organic Rankine cycle
GCR	Geometric concentration ratio
GMT	Greenwich mean time
CSP	Concentrated solar power
TES	Thermal energy storage
C	CPVT with cooling channel
NC	CPVT without cooling channel
CAPEX	Capital expenditure
DR	Diffuse irradiance
LST	Local solar time
LT	Local time
EoT	Equation of time
TC	Net time correction factor
LSTM	Local standard time meridian
HRA	Hour angle

Nomenclature:

W	Width $[\mathrm{m}]$
H	Height $[\mathrm{m}]$
M	Location of the mirrors $[\mathrm{m}]$
S	Distance of adjacent mirrors $[\mathrm{m}]$
fc	Focal length $[\mathrm{m}]$
K	Incidence angle modifier
Az	Azimuth angle $[°]$
Z	Zenith angle $[°]$
L	Length $[\mathrm{m}]$
A	Area $[\mathrm{m}^2]$
Q	Heat flux $[\mathrm{W}]$
T	Temperature $[\mathrm{K}]$
h	Heat transfer coefficient $\left[\frac{\mathrm{W}}{\mathrm{m}^2\mathrm{K}}\right]$
Nu	Nusselt number
k	Thermal conductivity $\left[\frac{\mathrm{W}}{\mathrm{mK}}\right]$
Dh	Hydraulic diameter $[\mathrm{m}]$
Re	Reynolds number
Pr	Prandtl number
t	Thickness $[\mathrm{m}]$
tr	Average spectral transmittance
f	Fraction of radiation absorbed
$\dot{m}$	Fluid mass flow rate $\left[\frac{\mathrm{kg}}{\mathrm{s}}\right]$
Cp	Specific heat capacity $\left[\frac{\mathrm{J}}{\mathrm{kgK}}\right]$
wt	Mass fraction
d	Day number of the year, ranging from 1 to 365
V	Velocity $\left[\frac{\mathrm{m}}{\mathrm{s}}\right]$

Greek letters:

δ	Tilt angle $[°]$
η	Efficiency
θ	Incidence angle $[°]$
σ	Stefan–Boltzmann constant $\left[\frac{\mathrm{W}}{\mathrm{m}^2\mathrm{K}^4}\right]$
ε	Emissivity
α	Elevation angle $[°]$
φ	Local latitude $[°]$
β	Declination of the sun $[°]$

Subscripts:

n	Number of primary mirror
ch	Channel
r	Receiver
opt	Optical
T	Transversal
L	Longitudinal
fl	Fluid
amb	Ambient
conv	Convection
cond	Conduction
rad	Radiation
ref	Reference
ap	Aperture
abs	Absorbed
atm	Atmosphere
th	Thermal
el	Electrical
NSE	Net solar-to-electric

Appendix A

A mathematical code is developed in Matlab to simulate the performance of the CPVT. The set of equations presented in the previous sections are solved using an iteration process. The flowchart of the model is illustrated in Figure A1. The output HTF temperature, location information, geometrical parameters, and fluid characteristics are used as input. The model uses the direct normal irradiance (DNI), global horizontal irradiance (GHI), wind speed, and ambient temperature from the NREL database [42]. The optical efficiency of the system is calculated using the location, solar angles, and geometrical data. Next, the variables to be determined are set up, and an iterative procedure based on energy balance is used. This process ends when all the energy and mass balance equations are satisfied. Lastly, the power and energy performance are determined.

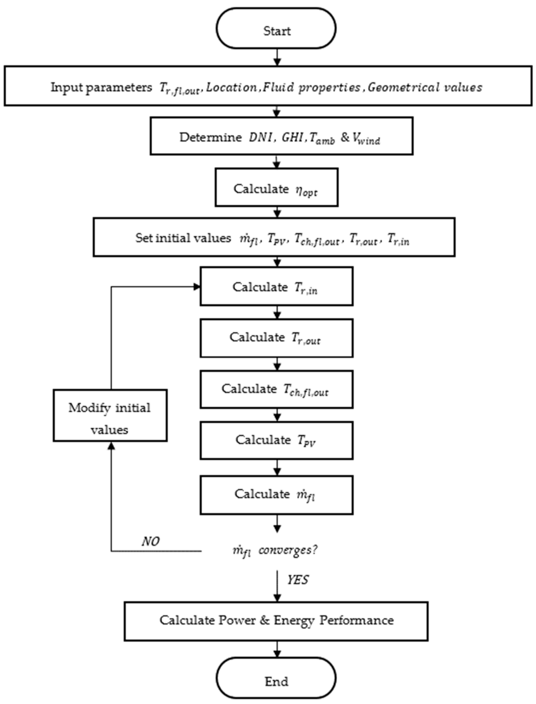

Figure A1. Flowchart of calculation model.

References

1. Han, X.; Tu, L.; Sun, Y. A spectrally splitting concentrating PV/T system using combined absorption optical filter and linear Fresnel reflector concentrator. *Sol. Energy* **2021**, *223*, 168–181. [CrossRef]
2. Mojiri, A.; Stanley, C.; Rosengarten, G. Spectrally Splitting Hybrid Photovoltaic/thermal Receiver Design for a Linear Concentrator. *Energy Procedia* **2014**, *48*, 618–627. [CrossRef]
3. Ramírez Quiroz, C.O.; Levchuk, I.; Bronnbauer, C.; Salvador, M.; Forberich, K.; Heumüller, T.; Hou, Y.; Schweizer, P.; Spiecker, E.; Brabec, C.J. Pushing efficiency limits for semitransparent perovskite solar cells. *J. Mater. Chem. A* **2015**, *3*, 24071–24081. [CrossRef]
4. Jarimi, H.; Lv, Q.; Ramadan, O.; Zhang, S.; Riffat, S. Design, mathematical modelling and experimental investigation of vacuum insulated semi-transparent thin-film photovoltaic (PV) glazing. *J. Build. Eng.* **2020**, *31*, 101430. [CrossRef]
5. Mujahid, M.; Chen, C.; Zhang, J.; Li, C.; Duan, Y. Recent advances in semitransparent perovskite solar cells. *InfoMat* **2021**, *3*, 101–124. [CrossRef]
6. Joshi, S.S.; Dhoble, A.S.; Jiwanapurkar, P.R. Investigations of Different Liquid Based Spectrum Beam Splitters for Combined Solar Photovoltaic Thermal Systems. *J. Sol. Energy Eng.* **2016**, *138*, 021003. [CrossRef]
7. Soule, D.E. Hybrid Solar Energy Generating System. 1987. Available online: https://www.osti.gov/biblio/5984591 (accessed on 28 May 2022).
8. Zhang, J.J.; Qu, Z.G.; Zhang, J.F. MCRT-FDTD investigation of the solar-plasmonic-electrical conversion for uniform irradiation in a spectral splitting CPVT system. *Appl. Energy* **2022**, *315*, 119054. [CrossRef]
9. Daneshazarian, R.; Cuce, E.; Cuce, P.M.; Sher, F. Concentrating photovoltaic thermal (CPVT) collectors and systems: Theory, performance assessment and applications. *Renew. Sustain. Energy Rev.* **2018**, *81*, 473–492. [CrossRef]
10. Ling, Y.; Li, W.; Jin, J.; Yu, Y.; Hao, Y.; Jin, H. A spectral-splitting photovoltaic-thermochemical system for energy storage and solar power generation. *Appl. Energy* **2020**, *260*, 113631. [CrossRef]
11. Liew, N.J.Y.; Yu, Z.; Holman, Z.; Lee, H.-J. Application of spectral beam splitting using Wavelength-Selective filters for Photovoltaic/Concentrated solar power hybrid plants. *Appl. Therm. Eng.* **2022**, *201*, 117823. [CrossRef]
12. Ju, X.; Xu, C.; Han, X.; Du, X.; Wei, G.; Yang, Y. A review of the concentrated photovoltaic/thermal (CPVT) hybrid solar systems based on the spectral beam splitting technology. *Appl. Energy* **2017**, *187*, 534–563. [CrossRef]
13. Sabry, M.; Gottschalg, R.; Betts, T.R.; Shaltout, M.A.M.; Hassan, A.F.; El-Nicklawy, M.M.; Infield, D.G. Optical filtering of solar radiation to increase performance of concentrator systems. In Proceedings of the Conference Record of the IEEE Photovoltaic Specialists Conference, New Orleans, LA, USA, 19–24 May 2002; pp. 1588–1591. Available online: https://www.scopus.com/inward/record.uri?eid=2-s2.0-0036957820&partnerID=40&md5=9aae59a3fe7add1b1f8cc02576b1774e (accessed on 29 May 2022).
14. Hangweirer, M.; Höller, R.; Schneider, H. Design and analysis of a novel concentrated photovoltaic–thermal receiver concept. *Jpn. J. Appl. Phys.* **2015**, *54*, 08KE01. [CrossRef]
15. Meraje, W.C.; Huang, C.-C.; Barman, J.; Huang, C.-Y.; Kuo, C.-F.J. Design and experimental study of a Fresnel lens-based concentrated photovoltaic thermal system integrated with nanofluid spectral splitter. *Energy Convers. Manag.* **2022**, *258*, 115455. [CrossRef]
16. Barthwal, M.; Rakshit, D. Holistic opto-thermo-electrical analysis of a novel spectral beam splitting-based concentrating photovoltaic thermal system. *J. Clean. Prod.* **2022**, *379*, 134545. [CrossRef]
17. Wang, G.; Ge, Z.; Lin, J. Design and performance analysis of a novel solar photovoltaic/thermal system using compact linear Fresnel reflector and nanofluids beam splitting device. *Case Stud. Therm. Eng.* **2022**, *35*, 102167. [CrossRef]
18. Su, B.; Wang, H.; Zhang, X.; He, H.; Zheng, J. Using photovoltaic thermal technology to enhance biomethane generation via biogas upgrading in anaerobic digestion. *Energy Convers. Manag.* **2021**, *235*, 113965. [CrossRef]
19. Su, B.; Han, W.; Qu, W.; Liu, C.; Jin, H. A new hybrid photovoltaic/thermal and liquid desiccant system for trigeneration application. *Appl. Energy* **2018**, *226*, 808–818. [CrossRef]
20. Rodrigues Fernandes, M.; Schaefer, L.A. Long-term environmental impacts of a small-scale spectral filtering concentrated photovoltaic-thermal system. *Energy Convers. Manag.* **2019**, *184*, 350–361. [CrossRef]
21. Anand, B.; Shankar, R.; Murugavelh, S.; Rivera, W.; Midhun Prasad, K.; Nagarajan, R. A review on solar photovoltaic thermal integrated desalination technologies. *Renew. Sustain. Energy Rev.* **2021**, *141*, 110787. [CrossRef]
22. George, M.; Pandey, A.K.; Abd Rahim, N.; Tyagi, V.V.; Shahabuddin, S.; Saidur, R. Concentrated photovoltaic thermal systems: A component-by-component view on the developments in the design, heat transfer medium and applications. *Energy Convers. Manag.* **2019**, *186*, 15–41. [CrossRef]
23. National Institute of Standards and Technology. Thermophysical Properties of Fluid Systems. Available online: https://webbook.nist.gov/chemistry/fluid/ (accessed on 14 May 2022).
24. Han, X.; Lu, L.; Yan, S.; Yang, X.; Tian, R.; Zhao, X. Stability, Thermal Conductivity and Photothermal Conversion Performance of Water-Based ZnO Nanofluids. *J. Therm. Sci.* **2021**, *30*, 1581–1595. [CrossRef]
25. Farzanehnia, A.; Sardarabadi, M. Exergy in Photovoltaic/Thermal Nanofluid-Based Collector Systems. In *Exergy and Its Application: Toward Green Energy Production and Sustainable Environment*; IntechOpen: Rijeka, Croatia, 2019. Available online: https://www.intechopen.com/chapters/66854 (accessed on 3 June 2022).
26. Hassani, S.; Taylor, R.A.; Mekhilef, S.; Saidur, R. A cascade nanofluid-based PV/T system with optimized optical and thermal properties. *Energy* **2016**, *112*, 963–975. [CrossRef]

27. Rungasamy, A.E.; Craig, K.J.; Meyer, J.P. A review of linear Fresnel primary optical design methodologies. *Sol. Energy* **2021**, *224*, 833–854. [CrossRef]
28. Zhu, Y.; Shi, J.; Li, Y.; Wang, L.; Huang, Q.; Xu, G. Design and thermal performances of a scalable linear Fresnel reflector solar system. *Energy Convers. Manag.* **2017**, *146*, 174–181. [CrossRef]
29. Said, Z.; Ghodbane, M.; Hachicha, A.A.; Boumeddane, B. Optical performance assessment of a small experimental prototype of linear Fresnel reflector. *Case Stud. Therm. Eng.* **2019**, *16*, 100541. [CrossRef]
30. Radwan, A.; Emam, M.; Ahmed, M. Chapter 2.15—Comparative Study of Active and Passive Cooling Techniques for Concentrated Photovoltaic Systems. In *Exergetic, Energetic and Environmental Dimensions*; Dincer, I., Colpan, C.O., Kizilkan, O., Eds.; Academic Press: Cambridge, MA, USA, 2018; pp. 475–505.
31. Wang, H.; Li, H.; Wang, L.; Bu, X. Thermodynamic Analysis of Organic Rankine Cycle with Hydrofluoroethers as Working Fluids. *Energy Procedia* **2017**, *105*, 1889–1894. [CrossRef]
32. An, W.; Li, J.; Ni, J.; Taylor, R.A.; Zhu, T. Analysis of a temperature dependent optical window for nanofluid-based spectral splitting in PV/T power generation applications. *Energy Convers. Manag.* **2017**, *151*, 23–31. [CrossRef]
33. Huaxu, L.; Fuqiang, W.; Dong, L.; Jie, Z.; Jianyu, T. Optical properties and transmittances of ZnO-containing nanofluids in spectral splitting photovoltaic/thermal systems. *Int. J. Heat Mass Transf.* **2019**, *128*, 668–678. [CrossRef]
34. Kincaid, N.; Mungas, G.; Kramer, N.; Wagner, M.; Zhu, G. An optical performance comparison of three concentrating solar power collector designs in linear Fresnel, parabolic trough, and central receiver. *Appl. Energy* **2018**, *231*, 1109–1121. [CrossRef]
35. U.S. Department of Energy. PROJECT PROFILE: Hyperlight Energy (CSP: COLLECTS). Available online: https://www.energy.gov/eere/solar/project-profile-hyperlight-energy-csp-collects (accessed on 30 May 2022).
36. IRENA. *Renewable Power Generation Costs in 2020*; International Renewable Energy Agency: Abu Dhabi, UAE, 2021. Available online: https://www.irena.org/publications/2021/Jun/Renewable-Power-Costs-in-2020 (accessed on 2 May 2022).
37. Liang, H.; Wang, F.; Yang, L.; Cheng, Z.; Shuai, Y.; Tan, H. Progress in full spectrum solar energy utilization by spectral beam splitting hybrid PV/T system. *Renew. Sustain. Energy Rev.* **2021**, *141*, 110785. [CrossRef]
38. Abarca, V. Energía Solar Térmica en la Industria: Potencial y Aplicaciones. Fundación de la Energía de la Comunidad de Madrid. Available online: https://www.fenercom.com/wp-content/uploads/2020/06/1_Energia_solar_termica_en_la_industria_potencial_y_aplicaciones_ASIT_fenercom-2020.pdf (accessed on 3 December 2022).
39. Thermal Hot Water Storage. Available online: https://ease-storage.eu/wp-content/uploads/2016/03/EASE_TD_HotWater.pdf (accessed on 5 December 2022).
40. Pratt & Whitney. Organic Rankine Cycle Power Generation. Available online: https://aeenewengland.org/images/downloads/AEE_ASHRAE_JointMeeting_March2013/orc_power_generation_pratt_and_whitney.pdf (accessed on 30 May 2022).
41. Rodrigues Fernandes, M.; Schaefer, L.A. Levelized cost of energy of hybrid concentrating photovoltaic-thermal systems based on nanofluid spectral filtering. *Sol. Energy* **2021**, *227*, 126–136. [CrossRef]
42. National Renewable Energy Laboratory (NREL). NSRDB: National Solar Radiation Database. Available online: https://nsrdb.nrel.gov/data-viewer (accessed on 27 November 2022).
43. Abedanzadeh, A.; Borgheipour, H.; Fakouriyan, S.; Torabi, F. Economic Evaluation of Supplying Commercial Thermal Load by a New CPVT System: A Case Study in Iran. *J. Appl. Comput. Mech.* 2021. [CrossRef]
44. Saudi Arabia, Country Profile 2019. Climate Transparency. Available online: https://www.climate-transparency.org/media/saudi-arabia-country-profile-2019#:~:text=This%20country%20profile%20is%20part,several%20studies%20by%20renowned%20institutions (accessed on 20 November 2022).
45. Ministerio de España. Factores de Emisión. Available online: https://www.miteco.gob.es/ca/cambio-climatico/temas/mitigacion-politicas-y-medidas/factores_emision_tcm34-446710.pdf (accessed on 30 May 2022).
46. Bloomberg. Lithium-Ion Battery Pack Prices Rise for First Time to an Average of $151/kWh. Available online: https://about.bnef.com/blog/lithium-ion-battery-pack-prices-rise-for-first-time-to-an-average-of-151-kwh (accessed on 10 December 2022).
47. National Renewable Energy Laboratory. Battery Lifespan. Available online: https://www.nrel.gov/transportation/battery-lifespan.html (accessed on 11 December 2022).
48. Sunrun. What Is the Life Expectancy of a Solar Battery? Available online: https://www.sunrun.com/go-solar-center/solar-articles/what-is-the-life-expectancy-of-a-solar-battery (accessed on 11 December 2022).
49. Six Years and 26 Batteries Later. Available online: https://itpau.com.au/knowledge/itps-battery-test-centre/#:~:text=A%20typical%20lithium%20ion%20battery,losses%20for%20lead%2Dacid%20systems (accessed on 11 December 2022).
50. An, W.; Zhang, J.; Zhu, T.; Gao, N. Investigation on a spectral splitting photovoltaic/thermal hybrid system based on polypyrrole nanofluid: Preliminary test. *Renew. Energy* **2016**, *86*, 633–642. [CrossRef]
51. How Hot Do Solar Panels Get and How Does It Affect My System? Solar Reviews. Available online: https://www.solarreviews.com/blog/how-hot-can-solar-panels-get (accessed on 13 December 2022).